

# A STUDY OF HEAT TRANSFER MECHANISMS AND FLOW CHARACTERISTICS FOR SINGLE RISING TAYLOR BUBBLES

Alex Scammell and Jungho Kim\*

Department of Mechanical Engineering, University of Maryland  
2181 Glenn L. Martin Hall, Building 088, UMD, College Park, MD 20740

\*email: kimjh@umd.edu

## ABSTRACT

The heat transfer enhancement due to slug flow has been widely studied both experimentally and numerically, yet identification of the main heat transfer mechanisms has been debated and little experimental evidence is available. In this work, an experimental study was undertaken to categorize the heat transfer distribution around a rising vapor Taylor bubble in co-current flow. It was seen that the largest heat transfer contribution was due to turbulent mixing in the bubble wake caused by vortex shedding at the bubble tail. Results for bubble velocity show modest agreement with correlations at low liquid velocities, but deviate as the liquid velocity increases. Thickness measurements for developed liquid films correspond well with correlations.

## KEYWORDS

Slug flow; Heat transfer; Infrared thermometry; Film thickness; Vortices

## 1. INTRODUCTION

Slug flow, characterized by elongated bubbles separated by liquid slugs, is frequently seen in pulsating heat pipes, microchannels, and in macro-scale channels at low vapor qualities. Vapor/gas slugs rising in a vertical column are called Taylor bubbles, and have been widely studied—a review of the literature prior to 1992 is given in Fabre and Line [1]. A review of some of the more recent work follows. Using a non-intrusive particle image velocimetry (PIV) technique, Nogueira et al. [2] tracked the flow field around rising bubbles within stagnant and flowing fluids of varying viscosities in a 32 mm inner diameter (ID) tube. Comparison of the experimental data to theoretical correlations found that both film velocity and thickness were under-predicted for film Reynolds numbers greater than 80. In a similar study, Nogueira et al. [3] observed the velocity patterns in the wake region of rising bubbles and related the wake flow pattern to the dimensionless parameter  $N_f$  for stagnant liquid conditions, and a modified Reynolds number for co-current flow.

Thickness measurements of the liquid film surrounding bubbles in horizontal microchannels were carried out by Han and Shikazono [4] using a laser focus displacement meter. They proposed correlations to predict the initial bubble film thickness using the collected experimental data. They later expanded their study to include the effect of evaporation and developed relations for calculation of the film thickness [5].

Accurate prediction of liquid film thickness and other bubble characteristics are crucial in the development of physics-based models for determining the heat transfer in slug flows. One such model by Jacobi and Thome [6] featured a two-zone representation of evaporation for elongated bubble flows where the regime was divided into a liquid slug region and a thin film region. It was suggested that the main mechanism of heat transfer was evaporation of the thin film trapped between the bubble and heated channel wall. This model was modified by Thome et al. [7] to include three zones: a liquid slug, an evaporating elongated bubble, and a vapor slug. As with the two-zone model, evaporation in the thin liquid film provided heat transfer several orders of magnitude higher than the single phase heat transfer due to the liquid slug.

A numerical investigation by Magnini et al. [8] predicted the shape, length, and local heat transfer of Taylor bubbles for boiling of several fluids in a 0.5 mm circular channel. They found that as the bubble entered the heated channel with a developing thermal boundary layer present, evaporation of the liquid film removed heat from the fluid and caused an increase in heat transfer over single-phase flow. The heat transfer coefficient rose monotonically from the bubble nose towards the tail, with the highest values occurring in the bubble wake region. Based on these results, they modified the three-zone model by Thome et al. [7] to include unsteady conduction through the liquid, yielding more agreeable results with the simulations.

Experimental heat transfer work to date has largely focused on the overall heat transfer enhancement of slug trains with respect to single phase flow, rather than on the mechanisms dictating heat transfer for each bubble. However, Hetsroni and Rozenblit [9] utilized an infrared technique to measure wall temperature profiles in non-evaporating air-water slug flow. The wall temperatures were observed to be uniform for passing liquid slugs, while faint higher temperature streaks were present on the wall when the bubbles passed. This suggests a higher heat transfer coefficient in the liquid slug than in the liquid film, but no quantitative data was presented.

To provide further clarification on the topic of slug flow heat transfer, an experimental study of single vapor Taylor bubbles rising in a vertical-upward, co-current flow is presented in this paper. Bubble shape, velocity, liquid film thickness and local heat transfer coefficient were the parameters of interest. The rising bubbles were analyzed using an infrared thermography technique [10], which allowed for the measurement of the local heat transfer coefficient as the bubble passed.

## **2. EXPERIMENTAL DESCRIPTION**

To characterize the heat transfer and dynamics of rising Taylor bubbles, a flow boiling experiment was conducted in which measurements of the local wall heat transfer and film thickness along with high speed images were obtained as single vapor bubbles of varying length rose in a vertical column containing upward flowing liquid. The study of single bubbles was chosen in lieu of bubble trains so flow conditions upstream and downstream of the bubbles could be measured, reducing the complexity in approximating the flow patterns and understanding the heat transfer profile around each bubble.

### **2.1. Flow Loop Description**

A schematic of the experiment flow loop can be seen in Figure 1. The working fluid was 3M Novec HFE 7100, a non-toxic, dielectric fluid with a boiling temperature of 57°C at 1 bar. HFE 7100 was pumped in a subcooled liquid state using a gear pump (Micropump L21755) as the flow rate was measured by a turbine flowmeter (Omega FLR1009). The liquid was heated to saturation at the test section inlet using a stainless steel preheater powered by a modified 1000W computer power unit (Silverstone SST-ST1000-P) and controlled using pulse width modulation via a LabVIEW™ interface.

The fluid then entered a section of the flow loop designed to create and release single Taylor bubbles. This section consisted of a bubble generation segment and a bypass segment connected at the downstream end by a three-way valve. To generate a bubble, the valve was set to divert the liquid flow through the bypass segment, while a wire heater evaporated liquid in the bubble generation segment. The bubble volume was varied by adjusting the power to the wire and the heating time. Once the desired bubble volume was generated, it was released by rotating the valve such that liquid was redirected through the bubble generation segment, pushing the bubble into the test section.

The bubble rose vertically into a 6 mm ID silicon test section positioned 200 mm downstream of the three-way valve where heat transfer measurements and flow visualization were made. Pressure taps were located at the inlet and outlet of silicon tube so differential and absolute pressures could be measured. The absolute

pressure transducer (Omega PX209-030A5V) was used to determine the saturation temperature of the fluid entering the test section. Immediately after leaving the heated silicon tube, the rising bubble passed through a glass adiabatic section (380 mm downstream of the three-way valve) where high speed video was obtained using a CMOS video camera (Phantom Miro eX4) at frame rates between 900 and 1200 frames per second. The high-speed visualization was used to determine the bubble length, study the dynamics of the tail, and analyze the bubble shape. A laser displacement sensor (Keyence LK-G5000) was used to measure the liquid film thickness around the bubble. The sensor was calibrated by measuring known thicknesses of HFE 7100 with a maximum uncertainty of 10  $\mu\text{m}$ .

Bubbles were condensed and the liquid subcooled in a counterflow heat exchanger where the secondary fluid was cold water provided by a recirculator (Neslab CoolFlow CFT-75). A bellows-type accumulator was included after the condenser with the dry side open to the room to maintain the system pressure at nominally 1 bar. Before re-entering the gear pump, the fluid was sent through a de-gassing membrane (Liqui-Cel SuperPhobic). A vacuum pump connected to the membrane for several hours prior to data being collected was used to degas the liquid.

Transducer data was collected using a 24-channel data acquisition system (Omega OMB-DAQ-3000) and recorded at a rate of 100 Hz through a LabVIEW<sup>TM</sup> interface. T-type thermocouples were installed at various locations in the flow loop for data analysis, calibration, and safety purposes. Uncertainty for the thermocouples was calculated to be  $\pm 0.12^\circ\text{C}$ . Heat transfer measurements and flow visualization were made using an IR camera (Electrophysics Silver 660M) at a frame rate of 246 Hz. Typical uncertainties for the major instrumentation and some of the reduced parameters are summarized in Table 1.

**Table I: Typical uncertainties for important system parameters and measurements.**

<b>Parameter</b>	<b>Typical Value</b>	<b>Uncertainty</b>
$G$ [ $\text{kg}/\text{m}^2\text{s}$ ]	44-146	5.2
$P_{\text{abs}}$ [millibar]	950-1050	1.3
$\delta$ [ $\mu\text{m}$ ]	235-400	10
$T_{\text{cam}}$ [ $^\circ\text{C}$ ]	34-80	0.14
$k_p$ [ $\text{W}/\text{m}\cdot\text{K}$ ]	0.12	0.01
$\alpha_{\text{Si}}$ [ $\text{m}^{-1}$ ]	144	6.5
$\alpha_p$ [ $\text{m}^{-1}$ ]	5277	192
$T_{\text{sat}}$ [ $^\circ\text{C}$ ]	56-60	0.14

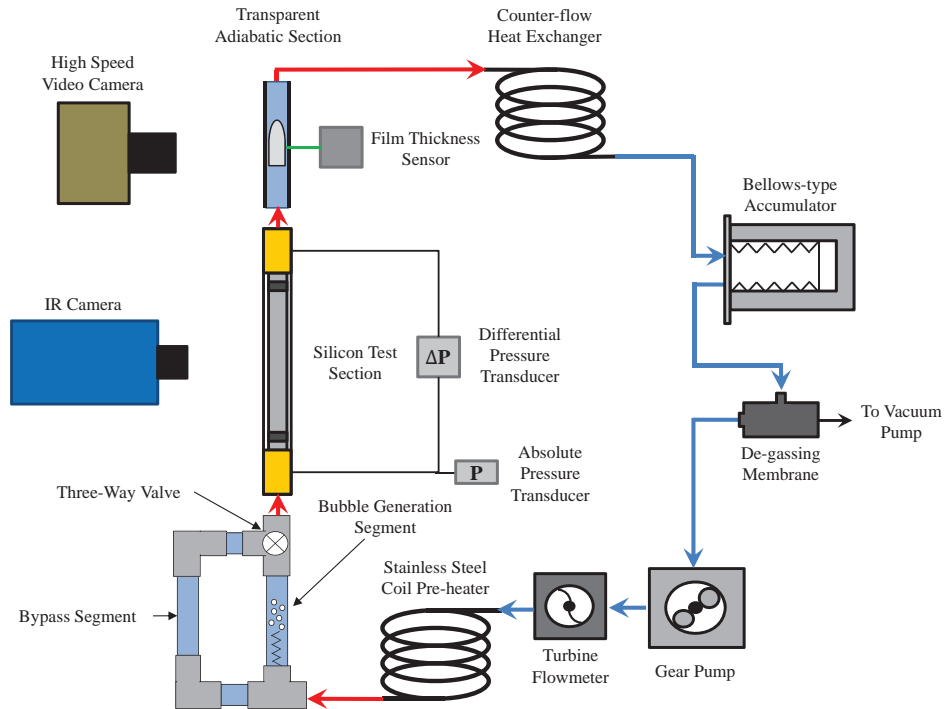


**Figure 1: Functional diagram for experimental test rig flow loop.**

## 2.1 IR Technique Description

Heat transfer measurements and flow visualization were obtained using an IR thermometry technique developed by Kim et al. [10] that takes advantage of the transparency of silicon in the mid-IR range (3-5  $\mu\text{m}$ ). HFE 7100 passed through the 6 mm ID (8 mm OD) single crystal silicon tube which was coated on the inner wall with a 57  $\mu\text{m}$  layer of polyimide tape ( $k=0.12$  W/m-K) as shown in Figure 2. One half of the inner circumference was then covered with an IR opaque paint containing carbon black (Nazdar GV111), which allowed an effective inner wall temperature to be measured through the silicon and polyimide layer. Two strips of the painted polyimide tape were also attached to the outer wall of the tube so the outer wall temperature could be measured.

A coupled conduction/radiation problem was solved which accounted for absorption, emission, and reflection of thermal energy from the layers and the surroundings to determine the temperature profile within the multilayer. The heat flux and heat transfer coefficient were then calculated for every camera pixel along the axial length of the tube. Details of the data reduction procedure can be obtained in Kim et al. [10]. To complement the heat transfer measurements, the flow was visualized using a set of six gold-plated mirrors (Figure 2) arranged such that flow visualization and heat transfer measurements could be captured using a single camera.

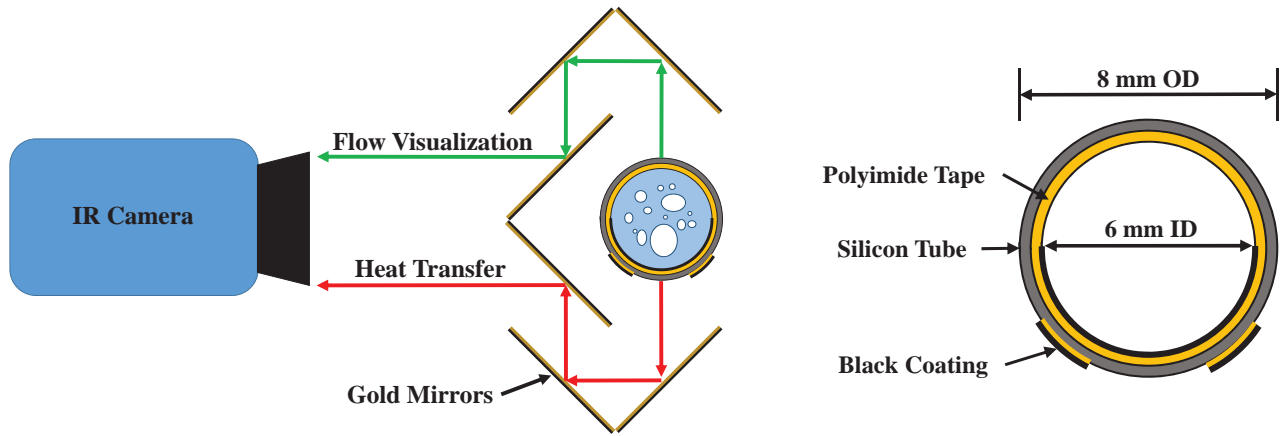


**Figure 2: Mirrors to provide simultaneous heat transfer measurements and flow visualization (left image), and cross-sectional view of silicon tube with coated polyimide tape (right image).**

Maximum uncertainties for the heat flux and heat transfer coefficient were estimated to be  $2.1 \text{ kW/m}^2$  and  $279 \text{ W/m}^2\text{K}$ , respectively. The uncertainty bars shown in heat transfer results include possible error associated with the determination of material optical properties, thicknesses, and camera temperature readings. Values for major sources of uncertainty were summarized in Table I.

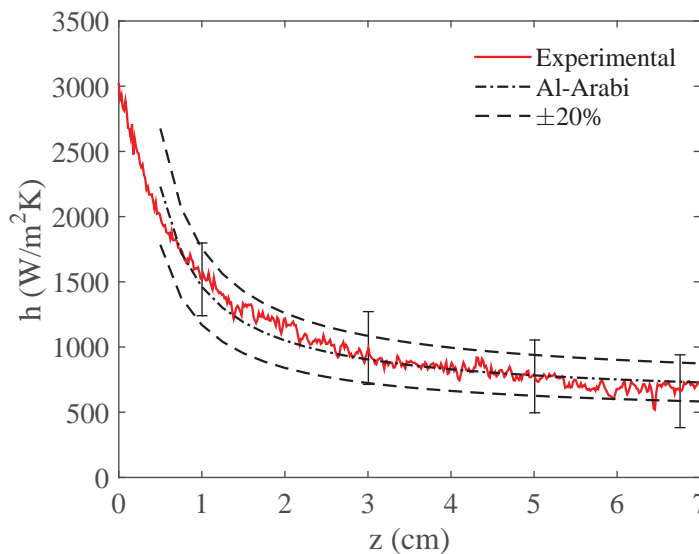


**Figure 3: Experimental heat transfer coefficient compared to the Dittus Boelter correlation with the Al-Arabi correction for the parameters: HFE 7100,  $Re=5545$ ,  $T_{sub}=20^\circ\text{C}$ ,  $q''=11 \text{ kW/m}^2$ .**

The IR thermography technique was validated through single-phase and two-phase testing in a vertical upward flow configuration. For single-phase flow, liquid passed through the heated silicon tube and the heat transfer coefficient along its length was measured. The experimentally measured heat transfer coefficient was compared to the Dittus-Boelter equation corrected for thermally developing flow at the beginning of the heated silicon tube using the factor proposed by Al-Arabi [11]. The experimental data shown in Figure 3 is in good agreement with the correlation. Two-phase validations were conducted by

comparing data obtained in the churn and annular flow regime to data collected by a group at IMFT in Toulouse, France using a test apparatus of different design but operated under similar conditions [12]. Figure 4 shows that data collected from both experiments are in agreement with each other as well as the correlations by Chen [13] and Cioncolini and Thome [14] at low vapor qualities.

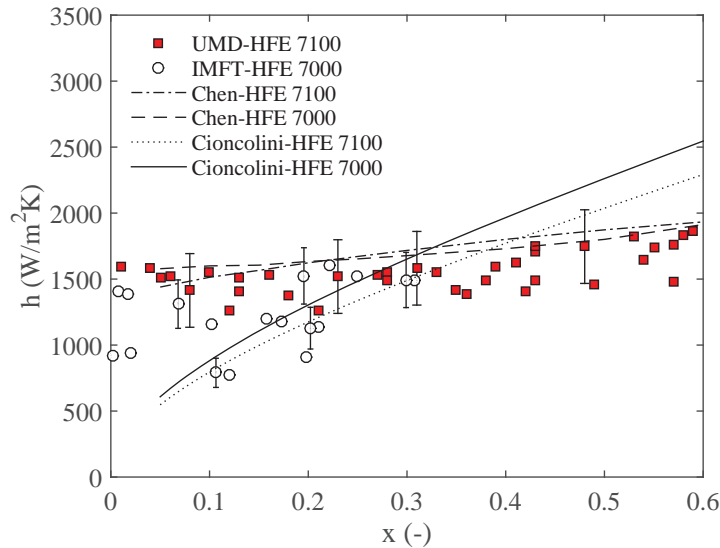


**Figure 4: Comparison of two-phase data collected by UMD and IMFT with similar experiments at conditions – UMD:  $G=100 \text{ kg/m}^2\text{s}$ ,  $q''=10 \text{ kW/m}^2$ ; IMFT:  $G=100 \text{ kg/m}^2\text{s}$ ,  $q''=9.8\text{-}36 \text{ kW/m}^2$ .**

### 3. RESULTS

#### 3.1. Bubble Dynamics

The bubble shape, velocity, and heat transfer characteristics were analyzed for a series of Taylor bubbles rising in fluid with co-current flow. Background liquid velocities within the test section were of the range  $31 \text{ mm/s} < U_L < 106 \text{ mm/s}$  ( $44 \text{ kg/m}^2\text{s} < G < 146 \text{ kg/m}^2\text{s}$ ). Once the generated bubbles were released using the three-way valve, heat transfer was measured as the bubble was tracked through the heated silicon test section. Film thickness measurements and high speed video were obtained in the adiabatic glass tube. Two representative bubbles are shown in Figure 5 to illustrate their general characteristics. The nose shape remained essentially the same for a given liquid velocity regardless of bubble length. The bubble tails were observed to oscillate, with frequency and amplitude varying with bubble length. Shearing of the bubble tail was not observed. As a result, all results presented are indicative of a single isolated Taylor bubble.

The bubble velocity was determined by identifying the bubble nose location on the infrared and high speed video as a function of time. A series of 15-20 bubbles were analyzed and averaged to obtain the bubble velocity at each liquid velocity. The bubble velocities were then compared to an equation proposed by Nicklin et al. [15]:

$$U_B = CU_L + U_{B,0} \quad (1)$$

where  $U_B$  is the bubble velocity,  $U_L$  is the measured bulk liquid velocity in the test section,  $C$  is a constant that defines the bubble drift velocity depending on the fluid velocity profile, and  $U_{B,0}$  is the bubble rise velocity in a stagnant fluid column determined from a graphical relation of White and Beardmore [16].

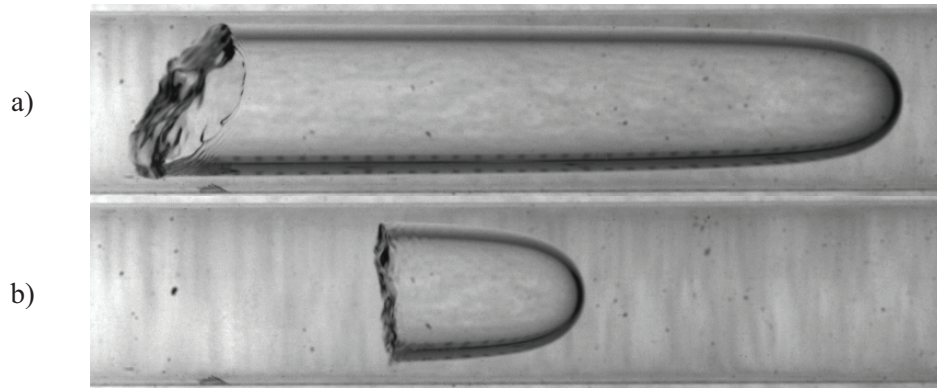


**Figure 5: Representative bubbles rising in co-current, saturated flow with  $U_L=72$  mm/s and lengths: a)  $L_B=33$  mm ( $L_B/D=5.5$ ), b)  $L_B=9$  mm ( $L_B/D=1.5$ ).**

Comparison of the experimental results to equation (1) is shown in Figure 6. The measured bubble velocities exhibit reasonable agreement with the correlation at liquid velocities smaller than 60 mm/s but show an increasing deviation as the liquid velocity increased above this value. The drift in bubble velocity from the prediction may be attributed to: 1) early transition to turbulent flow regime, or 2) underdevelopment of the liquid velocity profile at higher flow rates.

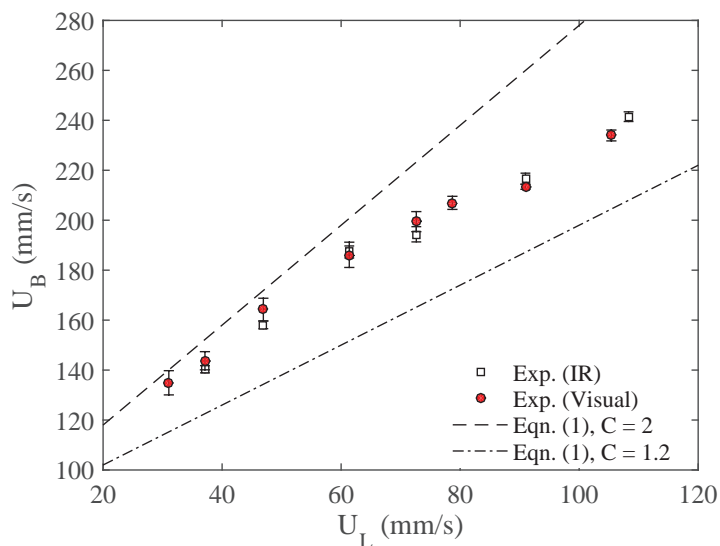


**Figure 6: Comparison of experimental bubble velocities (infrared and visual) to Nicklin's correlation.**

These values of  $C$  (2 and 1.2 for laminar and turbulent liquid flow, respectively) from equation (1) have traditionally been chosen to coincide with the ratio of the maximum velocity to the mean velocity within the tube. Nicklin et al. [15] found that  $C$  was approximately 1.2 at  $Re_L > 8000$ , but rose to 1.9 when the flow

was almost stagnant. Pinto et al. [17] also observed an evolution of  $C$  from 2 to 1.2 as the flow transitioned to turbulence, but noted that the  $Re_L$  at which this occurred was affected by the Weber number of the fluid. They proposed a correlation to predict  $C$  based on their experimental data and the data of Collins et al. [18]. Results for  $C$  from the current study are compared to the typical constants for laminar and turbulent flow ( $C=2$  and  $1.2$ ) in Figure 7 along with predictions by Pinto et al. [17]. Experimental values of  $C$  show a slight deviation from Pinto's correlation, especially at the low liquid Reynolds numbers. This is not surprising as the refrigerant fluid used here has rather different properties than water and aqueous glycerol solutions used in Pinto et al. [17], in particular much lower viscosity and surface tension.

It is also possible that the discrepancies in bubble velocity values from Nicklin et al. [15] occur because the flow is not yet fully developed at the measuring points in the experimental rig. When the bubble is released, it rises across the fluid coming from the bypass leg of the bubble generator, which forms a 90 degree elbow with the downstream upward section. The infrared measuring point is located 200 mm downstream, which corresponds to  $33D$ . The re-development length of the flow (which is not necessarily fully developed before the elbow) after the elbow increases with the Reynolds number. Hence, it is plausible that when  $G \leq 100$  kg/m<sup>2</sup>s, the distance between the elbow and the infrared measuring point is sufficient for the flow to become fully developed, thereby showing reasonable agreement with the correlation. Conversely, at larger mass flow rates, such a distance may be no longer sufficient, thus increasing deviation with the correlation.

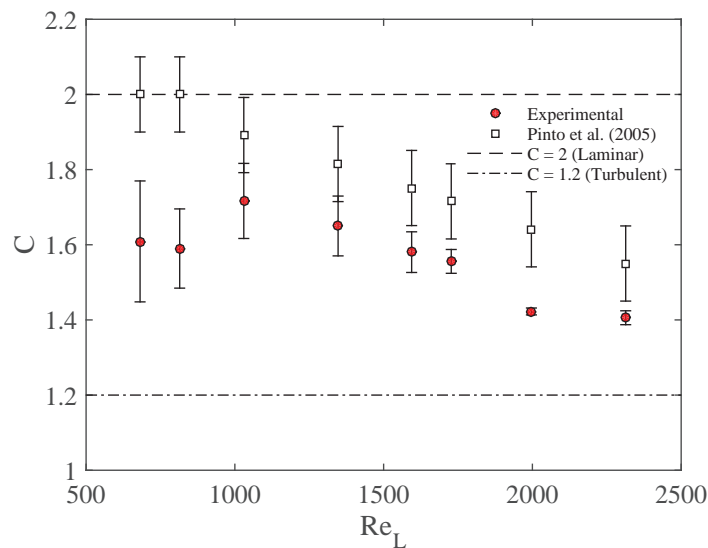


**Figure 7: Comparison of experimental values of  $C$  to predictions of Pinto et al. [17].**

In addition to determination of the rising bubble velocity, knowledge of the liquid film thickness is important if the film velocity and heat transfer are to be predicted. For this reason, film thickness measurements were made for each bubble as it passed, as shown in Figure 8. Due to the thickness sensor's operating principle of measuring reflected light from the bubble interface, data can only be collected once the film nears a fully developed state. A comparison of film thicknesses at the bubble tail as a function of bubble length for various liquid velocities is shown in Figure 9. The film thickness decreases with bubble length and approaches a constant value when the velocity profile within the film becomes fully developed. Campos and Carvalho [19] proposed a correlation to predict the distance ( $L_B^*$ ) from the bubble nose where the wall boundary layer reached the bubble interface:

$$\frac{L_B^*}{D} \approx \frac{\left[\left(\frac{g\delta^2}{2\nu}\right) + U_B\right]^2}{2gD} \quad (2)$$

Calculated values for  $L_B^*/D$  range from 13.8 to 16.1 for the experimental results depending on the bubble velocity. Nogueira et al. [2] found that at film Reynolds numbers ( $Re_{U_\delta} = (U_B - U_L)D/4\nu$ ) above approximately 80, the Campos and Carvalho correlation over-predicted their experimental results by as much as 30%. The current data shown in Figure 9 suggests  $L_B/D \sim 6$  is required for the film thickness to stabilize, a value not inconsistent with either prediction [2,19].

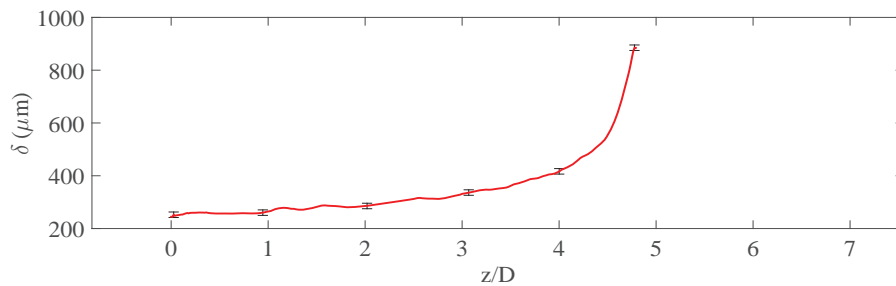
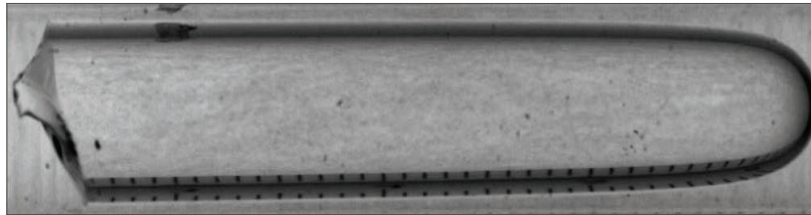


**Figure 8: Film thickness vs. axial distance from tail for bubble with  $L=37$  mm rising in co-current flow at  $U_L=46$  mm/s.**

Figure 9 also includes a comparison of the film thickness predicted using a theoretical relation developed by Brown [20] for a stabilized free-falling laminar film around a Taylor bubble rising in a co-current flowing liquid:

$$\delta = \left[ \frac{3\nu}{2g(R-\delta)} ((R-\delta)^2 U_B - R^2 U_L) \right]^{1/3} \quad (3)$$

It can be seen that once the liquid film becomes fully developed beyond approximately  $L_B/D=6$ , the agreement between experimental and predicted results is quite good. Very little variation in measured film thickness with liquid velocity is seen. This is supported by equation (3), which suggests the fully developed thicknesses differ by only  $10 \mu\text{m}$  (equal to the uncertainty of the measurements themselves) when bubble velocities for our test conditions are included.

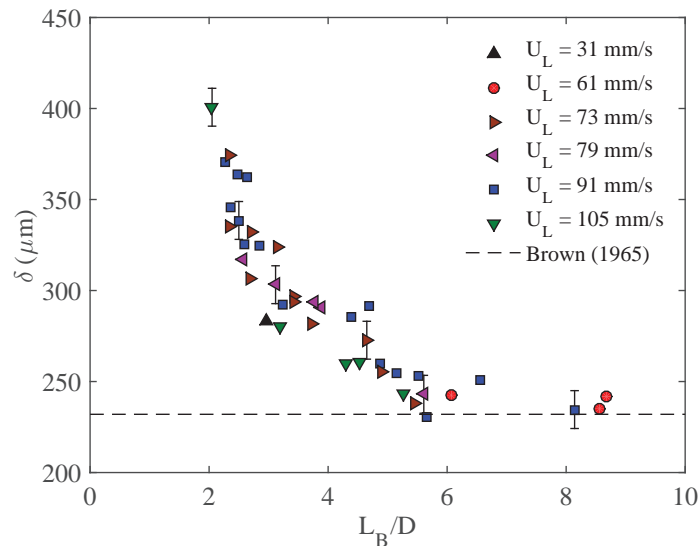


**Figure 9: Film thickness at the bubble tail vs. bubble length at various liquid velocities.**

### 3.2. Heat Transfer

In addition to the bubble shape and dynamics, heat transfer measurements were collected for each bubble as they passed through the test section. Steady-state, thermally developing flow was established within the heated section prior to each test to ensure reproducible boundary conditions. The heat transfer coefficient with time for a typical bubble passing a given position within the tube is shown on Figure 10. The heat transfer coefficient ahead of the bubble nose corresponds to single-phase flow. As the bubble passes, the flow is forced into the liquid film where it accelerates and the thermal boundary layer thins, leading to a small increase in the heat transfer coefficient. Vortices are generated when the downward moving film passes the bubble tail and interacts with the trailing liquid slug, inducing turbulence and a large spike in heat transfer. It is worth noting that, in the wake region behind the bubble, the flow field may be effectively turbulent even though the background liquid flow and the flow within the film are both laminar, as observed by Shemer et al. [21]. Once the turbulent mixing behind the bubble dies out, a thermally developing boundary layer is re-established and the heat transfer coefficient decays back to the single-phase value.

To better understand the mixing within the bubble wake, the heat transfer coefficient due to the vortices is shown in Figure 11. In this figure,  $z/D$  is the distance behind the bubble tail in a moving reference frame with the tail. Low heat transfer is observed immediately behind the tail as the liquid within the film diffuses into the trailing liquid. A large peak in the heat transfer follows due to impact of a vortex on the wall. Enhancements of over 1000% relative to single-phase flow were occasionally observed. It can also be seen that the highest vortex velocity is experienced just after the bubble passes, where the bubble film is impinging into the downstream fluid. Further work is ongoing to characterize the effect of the fluid and bubble mechanics on the local heat transfer profile.

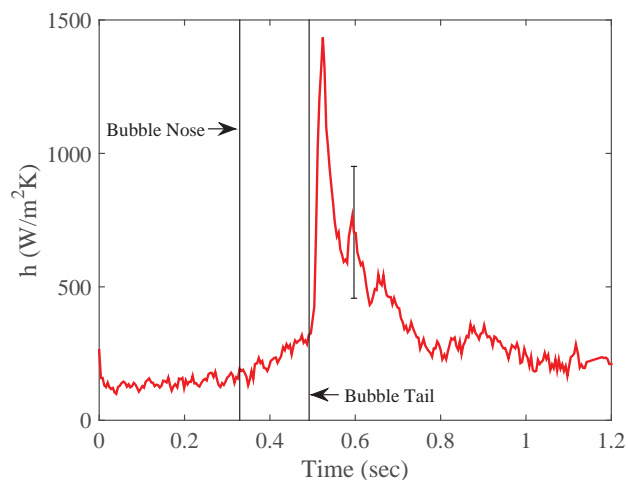


**Figure 10: Time trace of heat transfer coefficient for a bubble with  $L=21$  mm, rising in co-current flow at  $U_L=72$  mm/s, with  $q''=2400$  W/m<sup>2</sup>.**

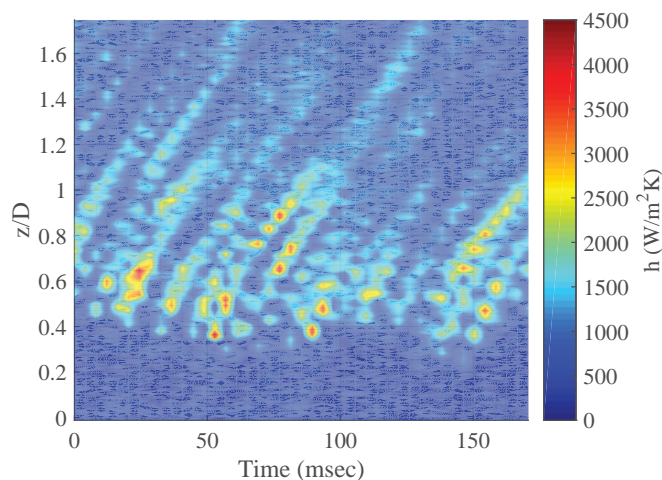


**Figure 11: Contour illustration of vortices being shed from a bubble with a moving reference frame located at the tail ( $z/D=0$ ) and rising in co-current flow at:  $U_L=72$  mm/s,  $q''=2.4$  kW/m<sup>2</sup>.**

#### 4. CONCLUSIONS

Experimental results and analysis illustrated that the dominant mechanism of heat transfer for rising vapor Taylor bubbles was turbulent mixing in the wake region caused by vortices shed at the bubble tail. Comparison of experimental bubble velocities to correlations showed reasonable agreement over the lower range of liquid velocities tested with a deviation at higher liquid velocities. This was attributed to either an early transition to turbulence or underdevelopment of the liquid flow under these conditions. Film thickness measurements were shown to compare well with classic correlations when the liquid film was fully developed. Building on these results, updated models for slug flow can be developed to provide more accurate heat transfer predictions.

#### NOMENCLATURE

##### General

D, tube diameter, mm  
 g, gravitational acceleration, m/s<sup>2</sup>  
 G, mass flux, kg/m<sup>2</sup>s  
 h, heat transfer coefficient, W/m<sup>2</sup>  
 k, thermal conductivity, W/m-K  
 L, bubble length, mm  
 P, pressure, bar  
 $q''$ , heat flux, W/m<sup>2</sup>  
 R, tube radius, mm  
 t, time, s  
 T, temperature, °C or K  
 U, velocity, m/s

##### Greek

$\alpha$ , absorptivity, m<sup>-1</sup>  
 $\delta$ , film thickness,  $\mu$ m  
 $\mu$ , dynamic viscosity, Pa  $\cdot$  s  
 $\nu$ , kinematic viscosity, m<sup>2</sup>/s  
 $\rho$ , density, kg/m<sup>3</sup>  
 $\sigma$ , surface tension, N/m

##### Subscripts

abs, absolute  
 B, bubble  
 cam, IR camera  
 L, liquid  
 p, polyimide  
 sat, saturation  
 Si, Silicon  
 V, vapor  
 w, wall  
 0, stagnant conditions

## ACKNOWLEDGMENTS

This work was supported by NASA Space Technology Research Fellowship NNX11AN49H and NASA grant NNX09AK39A. The authors would also like to thank Dr. Mirco Magnini (Heat and Mass Transfer Laboratory, EPFL) for many fruitful discussions regarding this work.

## REFERENCES

- [1] Fabre, J., and Line, A., 1992, "Modeling of Two-Phase Slug Flow," *Annu. Rev. Fluid Mech.*, **24**, pp. 21–46.
- [2] Nogueira, S., Riethmuller, M. L., Campos, J. B. L. M., and Pinto, a. M. F. R., 2006, "Flow in the nose region and annular film around a Taylor bubble rising through vertical columns of stagnant and flowing Newtonian liquids," *Chem. Eng. Sci.*, **61**(2), pp. 845–857.
- [3] Nogueira, S., Riethmuller, M. L., Campos, J. B. L. M., and Pinto, a. M. F. R., 2006, "Flow patterns in the wake of a Taylor bubble rising through vertical columns of stagnant and flowing Newtonian liquids: An experimental study," *Chem. Eng. Sci.*, **61**(22), pp. 7199–7212.
- [4] Han, Y., and Shikazono, N., 2009, "Measurement of the liquid film thickness in micro tube slug flow," *Int. J. Heat Fluid Flow*, **30**(5), pp. 842–853.
- [5] Han, Y., Shikazono, N., and Kasagi, N., 2012, "The effect of liquid film evaporation on flow boiling heat transfer in a micro tube," *Int. J. Heat Mass Transf.*, **55**(4), pp. 547–555.
- [6] Jacobi, A. M., and Thome, J. R., 2002, "Heat Transfer Model for Evaporation of Elongated Bubble Flows in Microchannels," *J. Heat Transfer*, **124**(6), p. 1131.
- [7] Thome, J. R., Dupont, V., and Jacobi, a. M., 2004, "Heat transfer model for evaporation in microchannels. Part I: presentation of the model," *Int. J. Heat Mass Transf.*, **47**(14-16), pp. 3375–3385.
- [8] Magnini, M., Pulvirenti, B., and Thome, J. R., 2013, "Numerical investigation of hydrodynamics and heat transfer of elongated bubbles during flow boiling in a microchannel," *Int. J. Heat Mass Transf.*, **59**, pp. 451–471.
- [9] Hetsroni, G., and Rozenblit, R., 2000, "Thermal patterns on a heated wall in vertical air-water flow," *Int. J. Multiph. Flow*, **26**(2), pp. 147–167.
- [10] Kim, T. H., Kommer, E., Dessiatoun, S., and Kim, J., 2012, "Measurement of two-phase flow and heat transfer parameters using infrared thermometry," *Int. J. Multiph. Flow*, **40**, pp. 56–67.
- [11] Al-Arabi, M., 1982, "Turbulent Heat Transfer in the Entrance Region of a Tube," *Heat Transf. Eng.*, **3**(3-4), pp. 76–83.
- [12] Narcy, M., Scammell, A., Colin, C., and Kim, J., 2014, "Flow Boiling Under Microgravity Conditions: Comparative study of two experimental data sets," *Proceedings of the 15th International Heat Transfer Conference, Kyoto*, pp. IHTC15–9072.
- [13] Chen, J. C., 1966, "Correlation for Boiling Heat Transfer to Saturated Fluids in Convective Flow," *Ind. Eng. Chem. Process Des. Dev.*, **5**(3), pp. 322–329.
- [14] Cioncolini, A., and Thome, J. R., 2011, "Algebraic turbulence modeling in adiabatic and evaporating annular two-phase flow," *Int. J. Heat Fluid Flow*, **32**(4), pp. 805–817.
- [15] Nicklin, D. J., Wilkes, J. O., and Davidson, J. F., 1962, "Two phase flow in vertical tubes," *Trans. Inst. Chem. Eng.*, **40**, pp. 61–68.
- [16] White, E. T., and Beardmore, R. H., 1962, "The velocity of rise of single cylindrical air bubbles through liquids contained in vertical tubes," *Chem. Eng. Sci.*, **17**, pp. 351–361.
- [17] Pinto, A. M. F. R., Coelho Pinheiro, M. N., Nogueira, S., Ferreira, V. D., and Campos, J. B. L. M., 2005, "Experimental Study on the Transition in the Velocity of Individual Taylor Bubbles in Vertical Upward Co-Current Liquid Flow," *Chem. Eng. Res. Des.*, **83**(9), pp. 1103–1110.
- [18] Collins, R., Moraes, F. F. De, Davidson, J. F., and Harrison, D., 1978, "The motion of a large gas bubble rising through liquid flowing in a tube," *J. Fluid Mech.*, **89**, pp. 497–514.

- [19] Campos, J. B. L. M., and Carvalho, J. R. F. G. De, 1988, "An experimental study of the wake of gas slugs rising in liquids," *J. Fluid Mech.*, **196**, pp. 27–37.
- [20] Brown, R. A. S., 1965, "The mechanics of large gas bubbles in tubes: I. Bubble velocities in stagnant liquids," *Can. J. Chem. Eng.*, **43**(5), pp. 217–223.
- [21] Shemer, L., Gulitski, a., and Barnea, D., 2007, "On the turbulent structure in the wake of Taylor bubbles rising in vertical pipes," *Phys. Fluids*, **19**(3), p. 035108.